Taylor & Francis
Taylor & Francis Group

Australian Journal of Mechanical Engineering

ISSN: 1448-4846 (Print) 2204-2253 (Online) Journal homepage: http://www.tandfonline.com/loi/tmec20

Helicopter gearbox bearing blind fault identification using a range of analysis techniques

N Sawalhi & R B Randall

To cite this article: N Sawalhi & R B Randall (2008) Helicopter gearbox bearing blind fault identification using a range of analysis techniques, Australian Journal of Mechanical Engineering, 5:2, 157-168

To link to this article: http://dx.doi.org/10.1080/14484846.2008.11464544

Helicopter gearbox bearing blind fault identification using a range of analysis techniques *

N Sawalhi † and RB Randall
School of Mechanical and Manufacturing Engineering, The University of New South Wales, Sydney

SUMMARY: *Vibration acceleration signals were obtained from an overload test of a Bell 206 helicopter main rotor gearbox in order to complete a blind bearing fault analysis where no knowledge of the fault was made available prior to the analysis. A range of diagnostic techniques was applied. These included power spectral density comparisons, constant percentage bandwidth (CPB) spectrum analysis, SK analysis to determine the frequency bands with maximum impulsiveness and to filter the signal to maximise that impulsiveness, and envelope analysis to determine the fault frequencies. Order tracking was used to compensate for speed fluctuations, while linear prediction using autoregressive models (AR) was used to remove the regular gear meshing contribution in the signals. As a result of applying these techniques, a fault in one of the planetary bearings was identified. A match with the cage frequency and the inner race ball pass frequency indicated deterioration associated with these components. Roller fault frequencies were not directly detected, but the fact that roller faults give a modulation at cage frequency shows that their effect was still detected. SK gave a good measure of the severity of the fault when compared to the amount of metal wear debris in the oil. Details of the test, as well as application of a statistical fault detection technique can be found in a companion paper submitted by the Defence Science and Technology Organisation (DSTO) Australia.*

1 INTRODUCTION

Many failures that occur in rotating components, like gears and bearings often show their signature in the vibration signal, and can be detected at an early stage. Monitoring those vibrations often requires an extensive interpretation by a trained diagnostician, due to the complexity of such systems (Forrester, 1991).

Helicopter transmission gearboxes have been investigated in detail to understand the types of baseline frequencies and failure indicators that can be detected by monitoring vibrations (McFadden & Smith, 1985; Lewicki & Coy, 1987). Those efforts resulted in a better understanding of the way in which different signals express themselves and mix with others, and led to the development of a variety of diagnostic and prognostic techniques (McFadden & Howard, 1999; Huff & Turner, 2003; Dempsey et al, 2004). In general, interpreting the vibration signal transmitted through such gearboxes often requires more than the traditional inspection of the time signal and/or its frequency content. This is due mainly to the existence of a large number of rotating components, all of which contribute and mix in different ways (Forrester, 1991), making it very hard to track changes in a certain component. A good example, which shows the difficulty of fault detection and diagnostics in helicopter transmission systems, is the case of a faulty bearing in a planetary gear. The fault signal has to travel through an indirect and time varying path to arrive at external measurement points. This varying transmission path and the strong contribution from gears, which spread all over the full acoustic frequency range, make it almost impossible to analyse the signal in the conventional ways used with bearings to extract the fault signature (Bonnardot et al, 2004).

Different techniques have been utilised for bearing diagnostics in such environments, aiming at separating the gear signals from the bearing ones. These include the use of synchronous averaging (McFadden & Howard, 1999), self-adaptive noise cancellation (SANC) (Ho & Randall, 2000), and discrete random separation (DRS) (Antoni & Randall,

* Reviewed paper originally presented at the First World Congress on Engineering Asset Management (1st WCEAM), Gold Coast, Australia, 2006.

† Corresponding author Nader Sawalhi can be contacted at n.sawalhi@unsw.com.au.

2004). Once the separation is achieved, envelope analysis (Ho & Randall, 2000; Darlow et al, 1974) which is a widely used technique for bearing analysis – is employed to extract bearing defect frequencies, thus indicating the source and the nature of the fault. However, as minor speed variation exists in practice, it is necessary to remove this variation and phase-lock the vibration signal to shaft speed. This is achieved through the use of order tracking, and is usually performed by re-sampling the vibration data at uniform rotational angles – using a tacho signal – rather than time based intervals (Forrester, 1991). In reference Bonnardot et al (2004) showed that this re-sampling can be achieved using the signal itself, and combined that with the use of self adaptive noise cancellation, which resulted in a clear identification of a ball fault in a planetary bearing and proved to be much more efficient than using SANC on its own. However, the selection of the frequency band for demodulation purposes (envelope analysis) was performed on the basis of trial and error, and needed to test more than one band to be able to detect the fault.

In this paper, different techniques are combined to provide an effective and automated extraction of a fault from a planetary bearing, which was blindly analysed from accelerometer signals measured at the helicopter transmission test rig facility at DSTO. The proposed algorithm starts by compensating for speed variations by re-sampling the signal synchronously with rotational speed using a tachometer signal. The re-sampled signal is then analysed using a newly developed technique for rolling element bearings (Sawalhi & Randall, 2005). This technique combines the use of autoregressive models, complex Morlet wavelet banks and spectral kurtosis (SK) (Antoni, 2006; Antoni & Randall, 2006) to automate the selection of the best band for envelope analysis.

The algorithm is taken a step further, by investigating its suitability for trend analysis, and possibly the prognosis of the fault. This is made possible by comparing the outcome of the algorithm (Spectral kurtosis evolution and filtered signals) with the amount of metal debris obtained from the test rig lubricant, and also by comparing constant percentage bandwidth (CPB) spectra at different stages of the fault.

2 EXPERIMENTAL WORK

Experimental data was obtained from a test performed in the DSTO, and was blindly analyssed for a defect in one of the bearings in the transmission system. The conditions for generation of the data included an overload test, which was carried out over different time intervals allowing the monitoring of fault development at different stages.

2.1 Bell 206 transmission description

The Bell 206-transmission system as shown in figure 1 is a two-stage reduction gearbox. The first stage consists of a spiral bevel pinion gear with (N_{pinion} = 19 teeth) driven by the input shaft from the engine side and rotating at a speed of (f_{input} = 100 Hz), which meshes with a bevel gear (N_{bevel} = 71 teeth). Triplex ball bearings and one roller bearing support the bevel pinion shaft. Duplex ball bearings and one roller bearing support the bevel gear shaft in an overhung configuration.

The second reduction stage is provided through a planetary mesh. The epicyclic gear system consists of a sun gear (N_{sun} = 27 teeth), splined to the bevel gear shaft, which in turn drives three planet gears (N_{planet} = 35 teeth). The planet gears mesh with a ring gear (N_{ring} = 99 teeth), which is attached to the top casing. Power is transmitted through the planet carrier, which is attached to the mast output shaft. The overall reduction ratio of the main transmission is (17.79:1) driving the output at (f_{out} = 5.73 Hz).

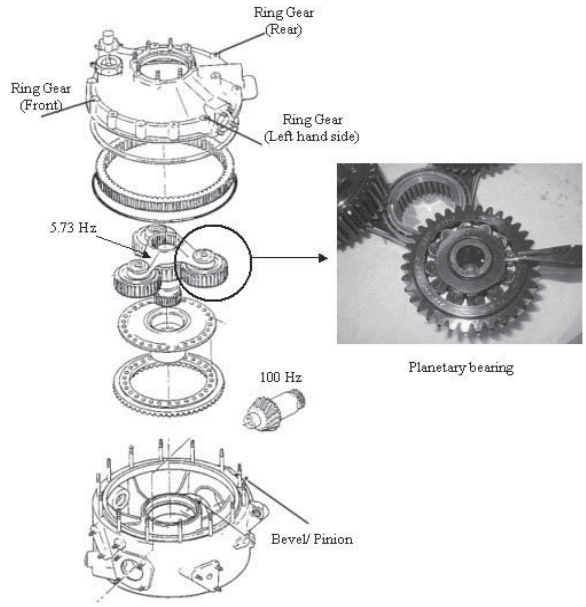

Figure 1: Bell 206 transmission and the planetary bearing.

Vibration data was collected from four accelerometers located on the transmission housing as shown in figure 1. Three of them were attached to the ring gear, measuring vibration at the second stage (planetary gears). The aim of the test was to initiate and propagate a non-seeded fault in the gearbox. In order to achieve the aim in a reasonable amount of time, the gearbox was run at 150 percent of its rated operating load, with periodic reductions in load to facilitate the recording of vibration signals. At a sampling frequency of 51.2 kHz, 30-second records were obtained at different stages of the fault. Each accelerometer is mounted so that its axis of measurement intersects the rotation axis of the shaft

at 90 degrees. In addition to the accelerometers, two tachometers were placed at the input and output shafts. For this analysis, only one accelerometer was used as the one that gave the best indication of the fault. This was the front accelerometer.

Debris was collected from the gearbox oil using an inline MetalSCAN unit. This was done in parallel with vibration measurements, and the cumulative mass was recorded against the test hour. Oil temperature was also monitored all the way through the whole test.

2.2 Expected frequencies

The vibration signal is expected to contain all frequencies due to meshing between the different sets of gears, their harmonics and sidebands. References Huff and Turner (2003), Lang (1999) give a complete description of computing those frequencies. This is adopted here for the same purpose, taking into consideration the differences in rotational speeds and the numbers of teeth on the different gears.

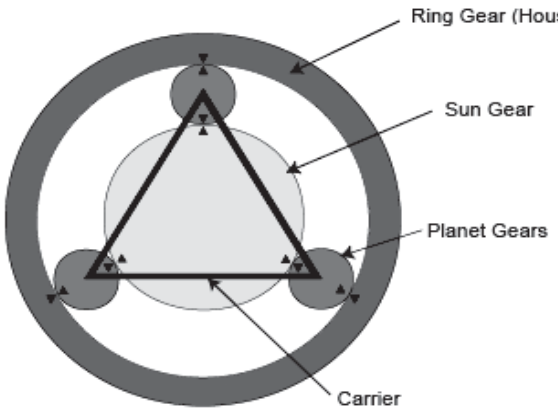

Figure 2: Elements of a simple planetary or epicyclic gear train (Lang, 1999).

Figure 2 shows a schematic presentation of the planetary gear system. The motion of such a system can be easily understood by a superposition analysis, which can be done in two sequential steps and summed to obtain the relative movements between the different components (Lang, 1999).

In the first step, the carrier (arm) is "locked" in position and the ring gear is free to rotate. The planet gear and the sun gear rotations are estimated based on that. In the second step all elements of the gear train are "locked" together and the entire assembly is rotated backwards until the ring gear is back to its original position. Summing those two actions provides the total rotations of all components. The relevant values for the system under investigation are shown in table 1.

Note that, as the planet gears and the carrier rotate in opposite directions, the net speed of a planet gear with respect to the carrier is the sum of the absolute speeds of the planet gear and the carrier. This is known as the spin frequency of the planetary gears, and can be alternatively calculated using equation (1).

$$f_{spin} = -\frac{N_{ring}}{N_{planet}} f_{out} \tag{1}$$

where the negative sign in equation (1) indicates that the planets spin in the opposite direction to the sun gear and the carrier. Calculated results showing shaft speeds and gear mesh frequencies in the Bell 206 transmission system are presented in table 2.

Table 1: Shaft speed estimation for different rotating parts.

Rotational frequency* (Hz) of:	Planet Gears f_{planet}	Sun gear f_{sun}	Gear carrier (Output shaft) f_{out}	Plant gear with respect to plant carrier (spin frequency) f_{spin}
	-10.48	26.76	5.73	-16.21

* Values estimated based on 100 Hz input shaft frequency.

Table 2: Gear mesh frequencies.

	Frequency of interest	**Hz**
Stage 1	Input shaft frequency	100.00
	Pinion Mesch frequency	1900.00
	Bevel Gear shaft speed	26.76
	Bevel Mesh frequency	1900.00
	Sun mesh frequency	722.54
Stage 2	Carrier frequency (output arm speed)	5.73
	Epicyclic mesh frequency	567.71
	Plant pass frequency	17.20

The same vibration signal will also contain frequencies resulting from bearings. Rolling element bearing frequencies are generated when a bearing begins to fatigue. These will be too weak to show in the early stages of the fault due to the high contribution from the gear meshing frequencies. For a fixed outer race (most common situation), the load direction is fixed with respect to the outer race, and equations (2 – 5), (Howard, 1994) are used to calculate the defect frequencies. Note that this is kinematically identical to the planet gears discussed above for a load angle $\alpha = 0$. The load angle is taken for the dominant load path, but actually varies for each rolling element, which is the reason for the random slip that always occurs. Thus, actual mean bearing frequencies typically differ from the theoretical ones by 1-2%, and the corresponding pulse period also varies randomly by about the same amount.

Inner Race Defect Frequency [BPFI]

$$f_{BPFI} = \frac{Nf_i\left(1+\frac{d}{D}\cos(\alpha)\right)}{2} \quad (2)$$

Outer Race Defect Frequency [BPFO]

$$f_{BPFO} = \frac{Nf_i\left(1-\frac{d}{D}\cos(\alpha)\right)}{2} \quad (3)$$

Cage Rotational Frequency relative to outer race (fundamental train frequency) [FTF]

$$f_{FTF} = \frac{f_i\left(1-\frac{d}{D}\cos(\alpha)\right)}{2} \quad (4)$$

Ball/Roller rotational speed around its axis (ball/roller spin frequency) [BSF]

$$f_{BSF} = \frac{f_i}{2}\frac{D}{d}\left(1-\left(\frac{d}{D}\cos(\alpha)\right)^2\right) \quad (5)$$

where N is the number of rolling elements, d and D are the rolling element diameter and the pitch diameter of the bearing respectively. f_i is the rotational speed of the inner race (shaft speed). α is the contact angle (from the radial).

Planetary bearings (figure 1) represent a special case, as the bearing is attached to the planet gear on its outer race, and to the carrier on its inner race, which means that both races will be rotating. Equations (6-10) are used to calculate the defect frequencies for the planetary bearings. Note that the load direction in the planetary bearings is fixed with respect to the inner race rather than the outer race (FTF is calculated as the cage speed relative to the inner race (carrier)), so that it is BPFO that is modulated by passage through the load zone, rather than BPFI as in the normal case.

Inner Race Defect Frequency [BPFI]

$$f_{BPFI} = \frac{N(f_{planet}-f_{out})\left(1+\frac{d}{D}\cos(\alpha)\right)}{2} \quad (6)$$

Outer Race Defect Frequency [BPFO]

$$f_{BPFO} = \frac{N(f_{planet}-f_{out})\left(1-\frac{d}{D}\cos(\alpha)\right)}{2} \quad (7)$$

Cage Rotational Frequency (absolute)

$$f_{cage} = \frac{f_{planet}\left(1-\frac{d}{D}\cos(\alpha)\right)}{2} + \frac{f_{out}\left(1+\frac{d}{D}\cos(\alpha)\right)}{2} \quad (8)$$

Cage Rotational Frequency relative to inner race (carrier) [FTF]

$$f_{FTF} = \frac{(f_{planet}-f_{out})\left(1+\frac{d}{D}\cos(\alpha)\right)}{2} \quad (9)$$

Ball/Roller rotational speed relative to both races (ball/roller spin frequency) [BSF]

Table 3: Bearing defect frequencies.

	Shaft speed (Hz)	**(BPFI) (Hz)**	**(BPFO) (Hz)**	**(FTF) (Hz)**	**(BSF) (Hz)**
Triplex bearing – input pinion	100.00	822.72	577.28	41.23	276.43
Roller bearing – input pinion	100.00	616.58	383.42	38.34	202.79
Bearing lower mast	26.76	273.63	208.85	11.56	96.45
Duplex bearing, input gear shaft – lower support	26.76	369.22	299.80	11.99	127.55
Duplex bearing, input gear shaft – upper support	26.76	356.68	285.57	11.90	59.85
Planetary bearings		117.72	76.95	9.81	37.04

$$f_{BSF} = \frac{f_{planet} - f_{out}}{2}\frac{D}{d}\left(1-\left(\frac{d}{D}\cos(\alpha)\right)^2\right) \quad (10)$$

where N is the number of rolling elements, d and D are the rolling element diameter and the pitch diameter of the bearing respectively. f_{planet} and f_{out} are the rotational speeds of the planetary gears and the output shaft (carrier) as in table 1. $\boldsymbol{\alpha}$ is the contact angle (from the radial).

Table 3 presents the theoretically calculated defect frequencies for bearings in the Bell 206 transmission system for $\boldsymbol{\alpha} = 0$.

3 DATA PROCESSING AND FAULT DIAGNOSTICS

The data from the accelerometers was processed in a number of sequential steps as shown in the block diagram of figure 3. The logic and ideas behind each processing step are as follows:

- Minimising the speed fluctuations that may exist in the transmission system. As has been indicated in the Introduction, the system under consideration contains a large number of rotating components, which all contribute to the vibration signal. Although the system in general runs at a nominal constant speed, it will exhibit minor speed variation in practice. For this reason, sampling of the vibration data is performed at rotational rather than time-based intervals (Forrester, 1991). This angular resampling (also known as order tracking) will force the gear signal to be deterministic and is done here using the tacho signal.
- Separating bearing signals from gear signals and pre-whitening. This is done using autoregressive models (AR), with the aim of analyzing the residual signal of the model (the so-called pre-whitened signal). The use of this signal in further processing steps, is more favourable than the use of the original signal (order tracked), and proved to give better results for the spectral kurtosis analysis (Wang & Wong, 2002).
- Searching for an optimum band for demodulation purposes. This is done using complex Morlet wavelets. These are used as a filter bank with constant proportional bandwidth (uniform resolution on a logarithmic frequency scale). Different banks are used to select the best filter for the envelope analysis as the one that maximises the SK (Antoni, 2006; Antoni & Randall, 2006).
- Extracting bearing defect frequencies and determining the source of the fault.

For the sake of diagnostics, only the result from the last measurement is discussed here, while more discussion is given on the fault in its different stages in the prognostic section. A depiction of the first 8930 samples (174.36 ms) representing the first rotation of the carrier (5.73 Hz) is given in figure 4. With a kurtosis (equation (11) value of -0.61 (platykurtic: negative kurtosis value (Joanes & Gill, 1998)) it is very difficult to recognise any impacts in the time domain signal. This is further investigated by examining the power spectral density (PSD) of the signal as shown in figure 5, which shows how the harmonics of the gear mesh frequencies (two families) dominate the spectrum, and can be seen over the whole useful range of the signal (to 20 kHz).

$$\text{Kurtosis} = \frac{\frac{1}{N}\sum_{i=1}^{N}(x(i)-\bar{x})^4}{\sigma^4} - 3 \quad (11)$$

where $x(t)$ is the digitised measured vibration signal, N is the number of samples and $\boldsymbol{\sigma}$ is the standard deviation and is given in equation (12). The "minus 3" at the end of equation (11) is often explained as

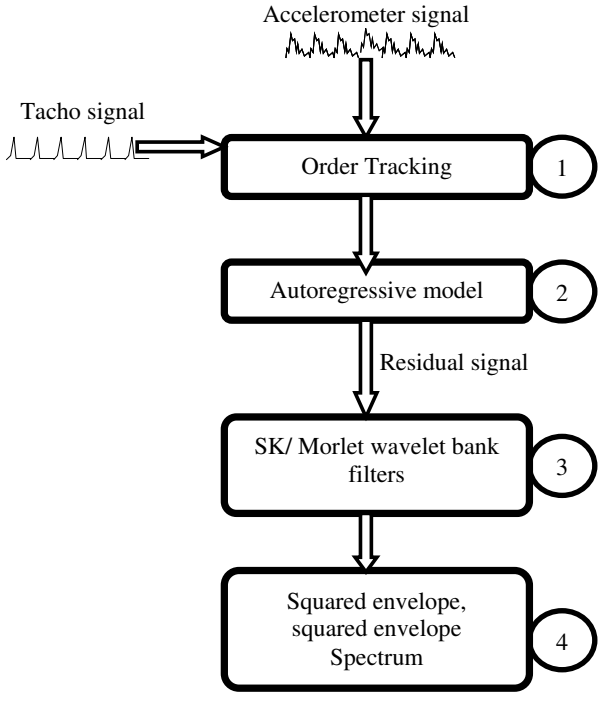

Figure 3: Block diagram presentation of signal processing steps.

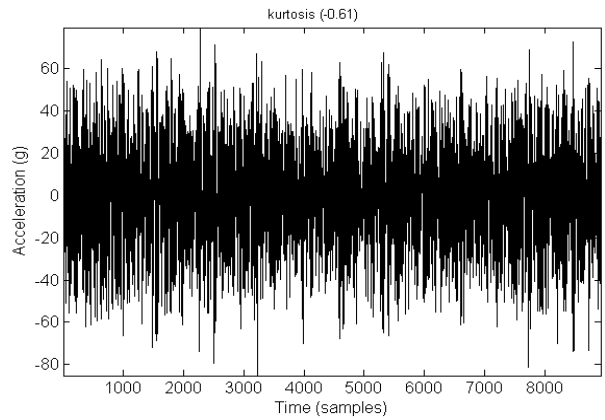

Figure 4: Accelerometer signal representing 1 rotation of the carrier.

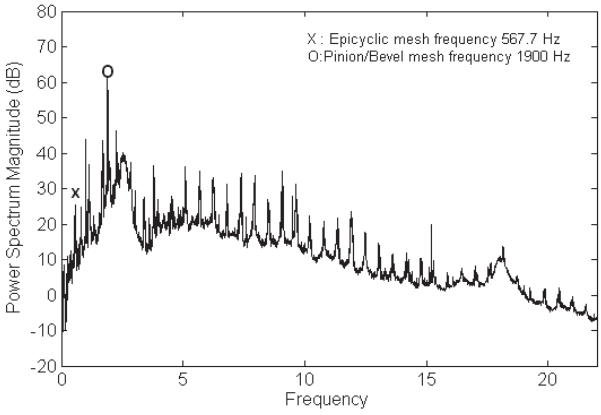

Figure 5: Power spectral density of the raw signal.

a correction to make the kurtosis of the normal distribution equals to zero.

$$\sigma = \sqrt{\frac{1}{N}\sum_{i=1}^{N}(x(i)-\bar{x})^2} \qquad (12)$$

3.1 Order tracking

Order tracking is a way of ensuring the deterministic property of the gearmesh signal while facilitating its treatment and interpretation in further steps of the analysis. Order tracking in concept is based on re-sampling the signal in the angular domain rather than the time domain. This can be done either by using hardware (phase-locked frequency multiplier), or by digitally re-sampling the signal with the aid of a tachometer signal (Forrester, 1991). In this study, all order tracking was performed using a digital re-sampling technique, where both the vibration signal and the tachometer signal were sampled simultaneously using a fixed time-based sampling frequency. Matlab® code was used for this purpose and included the use of a cubic spline interpolation of the vibration signal to calculate the values at the required sample points, based on the tachometer signal.

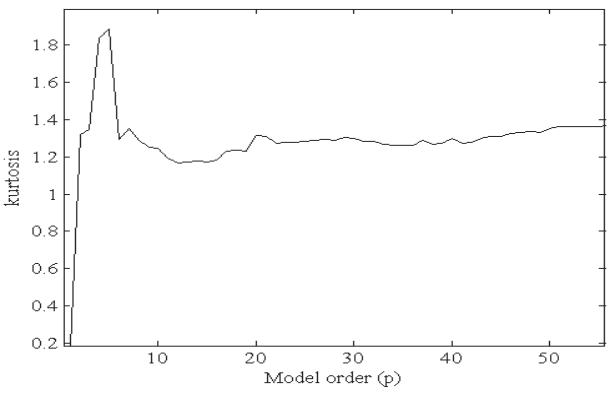

Figure 6: Kurtosis of residual signals for different model orders.

3.2 Linear prediction filtering and pre-whitening based on autoregressive modelling

Having obtained an order-tracked signal, with a deterministic gearmesh contribution, autoregressive models (AR) are used next with two main aims. The first is to remove gear contributions from the signal. This will result in the separation of the signal into two main parts, namely, a deterministic part (AR fitted signal – containing the gearmesh contribution) and a noise part (containing additive white noise and nonstationarities (impulses)). Because of the randomness referred to above, the bearing signals are contained in this part (Ho & Randall, 2000). The second aim from using AR models is pre-whitening. The noise part of the AR model is close to that of a white noise (power spectral density changes with frequency are very small), as it is made up of impulses and additive white noise. This has the advantage of solving an anomaly in the SK, and gives better results when used prior to the application of the SK (Wang & Wong, 2002).

In the process of designing an AR filter for linear prediction, a value of the signal at time index k is normally based upon a linear combination of prior values, according to equation (13) (Sawalhi & Randall, 2005):

$$x_k = -\sum_{i=1}^{p} a_i x_{k-i} + \varepsilon_k \qquad (13)$$

where the a_i are the autoregressive coefficients and ε_k is the residual error. The residual error ε_k (difference between the actual signal and the AR prediction) has an almost white spectrum, but can be made up of stationary noise and impulses.

The AR filter as described by equation (13), well predicts the deterministic pattern of the signal but is not capable of adapting to the sudden impulses caused by a localised fault. As a consequence, the

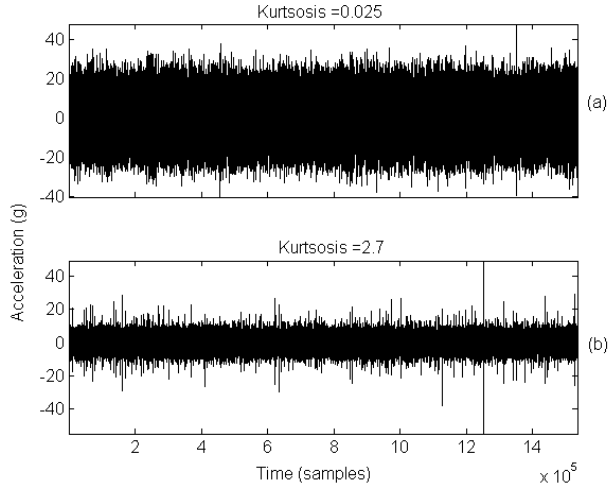

Figure 7: (a)Initially processed signal by ordertracking (b) AR (5) residual signal.

fault impulses will be left in the residual ε_k of the AR filter. If SK is applied on the residual signal, high SK values and a clearer extraction of fault impulses are obtained. Several criteria are in place to select the optimum model order, such as the Akaike Information Criterion (AIC) (Akaike, 1969), however as our main objective of using the AR technique for rolling element bearings resides in separating the impulses from the original signal, we find it intuitive to base the order selection criterion on maximising the kurtosis of the residual signal, which as has been indicated earlier, contains both the impulses and the stationary noise. The optimum model order p should be less than the spacing between two consecutive impulses, as this guarantees that the model does not adapt to the impacts as being a part of the deterministic signal and that they will be contained in the residual signal.

The optimum order for the AR model based on maximising the kurtosis of the residual signal is plotted in figure 6. It clearly shows that a filter length of five samples would be optimum and is preferred for a better extraction of impacts hidden in the system.

Figure 7 shows the effect of using a linear prediction filter and the benefits of analysing the residual signal rather than the raw signal. Impulses throughout the signal can be seen very clearly in the residual signal (b) when compared to signal (a) from the same figure. The passage of the planet gears can also be seen clearly (three bursts of increased amplitude in one rotation) when inspecting one rotation of the carrier as presented in figure 8. Other impulses do exist in the signal and will require further analysis to determine the source. A final point to mention in this regard is the increase of the kurtosis value from– 0.61 (in the order-tracked signal) to about 2.7 in the residual signal.

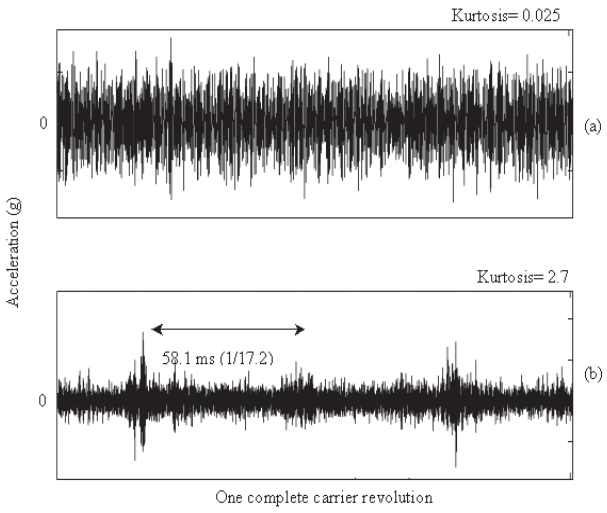

Figure 8: Zoom-in views (one rotation of the carrier) showing the effect of using an AR linear prediction filter for signal separation, (a) Order tracked signal, (b) Residual signal.

3.3 Automated envelope analysis using spectral kurtosis and complex morlet wavelet filter banks

The presentation of this section is based on what has been presented in (Sawalhi & Randall, 2005), in which Sawalhi and Randall used different filter banks constructed using Complex Morlet wavelets to select the best filter for the envelope analysis in terms of centre frequency and bandwidth – as the one that maximises the SK. This approach proved to be well suited for the purpose of rolling element signal analysis due to:

- The use of wavelets being more favourable than the STFT (short time Fourier transform) as the duration of the wavelet varies inversely with frequency corresponding to constant relative damping.
- The choice of complex Morlet wavelets helps to design a filter, which acts as a "matched filter" to condition transient signals in the data.
- The complex wavelets help detect transients in a uniform manner regardless of their phase.

The complex Morlet wavelet is defined in the time domain as a complex exponential wave multiplied by a Gaussian function, and has the shape of a Gaussian function in the frequency domain as follows:

$$\psi(t) = \frac{\sigma}{\sqrt{\pi}} e^{\sigma^2 t^2} e^{i2\pi f_o t} \tag{14}$$

$$\Psi(f) = \Psi^*(f) = e^{-(\pi^2/\sigma^2)(f-f_0)^2} \tag{15}$$

where $\Psi(f)$ is the Fourier Transform of ψ(t). Since $\Psi(f)$ is real, $\Psi(f) = \Psi(f)$, where * denotes the complex conjugate. f_o is the centre frequency of the window and σ determines its width. Since the real and

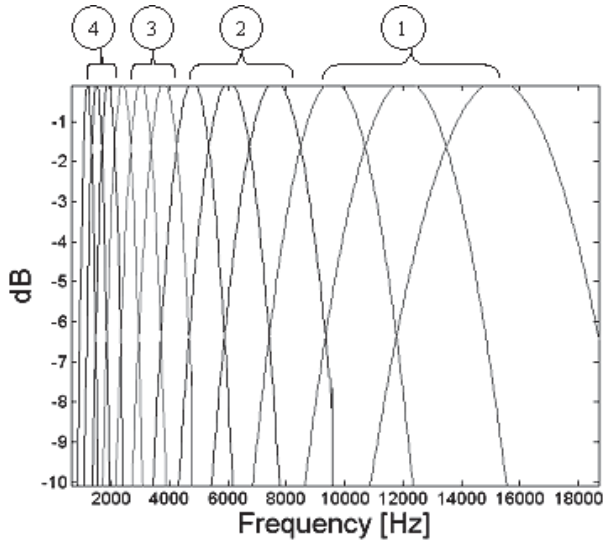

Figure 9: The coarse filter bank with three filters/octave filter bank covering 4 octaves.

imaginary parts of $\psi(t)$ are Hilbert transforms, it is analytic and its Fourier transform $\Psi(f)$ is one-sided with positive frequencies only.

The advantage of the complex Morlet wavelets, compared with the real version using windowed cosines, is that the imaginary parts (sines) have their maximum when the cosines have zero crossings, so that the squared amplitude of the wavelet coefficients is not sensitive to the phasing of local features in the time signals.

To optimise the use of complex Morlet wavelets as a filter bank, and to gain a balanced representation of the signal in time and frequency domains, a few banks with different numbers of filters per octave eg (3,6,12,24) or (2,4,8,16) were suggested to decompose the signal. In order to gain efficiency, the number of octaves covered in each bank can be reduced as the number of filters per octave is increased, as the coarser analysis gives an indication of the frequency bands with the highest impulsiveness. Moreover, filters for lower octaves can be derived by progressively down-sampling the higher octave filters by factors of 2, which accelerates the analysis. Figures 9 and 10 show two filter banks constructed using complex Morlet wavelets. A coarse one (3 filters/octave) spreading over 4 octaves is shown in figure 9 and a fine one (12 filters/octave) over one octave is presented in figure 10.

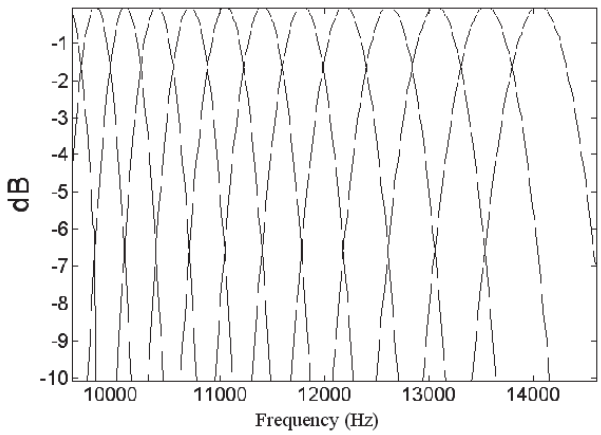

Figure 10: The fine filter bank covering twelve filters/octave filter bank covering 1 octave.

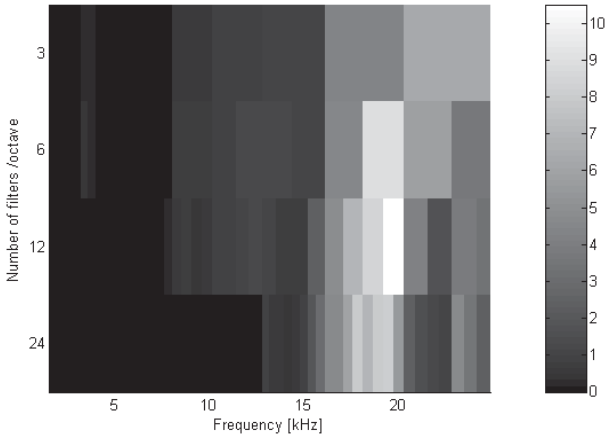

Figure 11: Image presentation of the SK variation for 4 filter banks; namely (3,6,12,24) filters/octave.

Once the filters are constructed, the signal can then be decomposed correspondingly. This is easily performed by multiplying the FFT of the signal by each row of the filter bank matrix, then by performing the IFFT to obtain the wavelet coefficients (complex values) (Sawalhi & Randall, 2005). The multiplication of the wavelet coefficients by their complex conjugate in fact gives the squared envelope of the filtered signal. If $y = |x|^2$ is the squared envelope signal, then the kurtosis corresponding to y can be calculated using equation (16), to give a single value for each filter.

$$kurtosis(y) = \frac{mean(y^2)}{(mean(y))^2} - 2 \qquad (16)$$

The value 2 is subtracted here, to obtain a value of zero for the squared envelope of Gaussian noise (Antoni, 2006). The best filter is chosen as the one that gives the highest value of kurtosis, ie maximising the SK from the squared envelope.

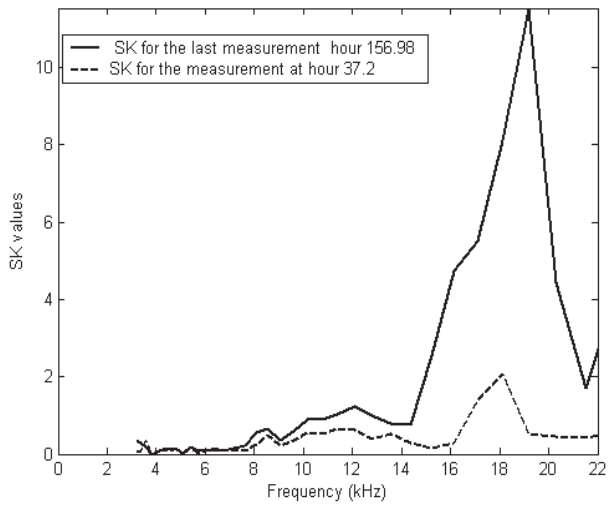

Figure 12: SK variation between first measurements at hour 37.2(dotted) and last measurement at hour 156.98.

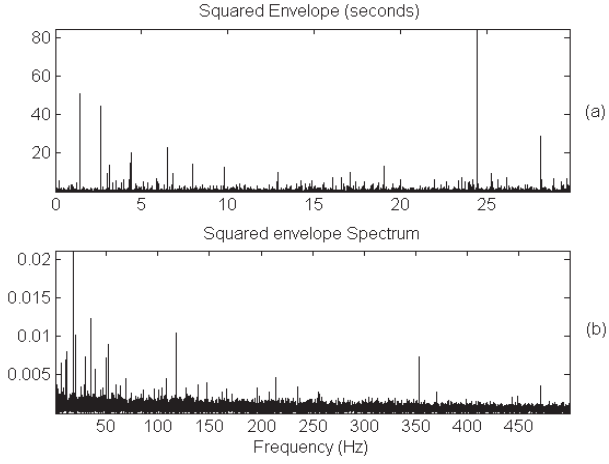

Figure 13: SK automated envelope analysis (a) squared envelope and (b) squared envelope spectrum.

After processing the residual signal (figure 7b) using the set of filter banks described, the result is plotted in figure 11 as an image, whose rows represent the filter banks (3,6,12,24 filters/octave), and columns represent the filters in each bank. The values assigned to each slot (filter) are the kurtosis of the squared envelope signal for that specific filter in the bank, and were calculated as shown in equation (16). The highest kurtosis indicates the optimum slot (filter) for the purpose of envelope analysis. The maximum SK was obtained using 12 filters/octave (centre frequency of 18,800 Hz and bandwidth 1175 Hz).

To gain more insight into the excitation across the frequency range, the SK is plotted in figure 12 using a bank of 12 filters/octave, which gave highest values for SK as inferred from figure 11. SK is plotted for the first and final measurements, showing the variation in SK values as well as the excited bands between the start of the test and the time it was stopped.

The squared envelope and the envelope spectrum for the last measurement are presented in figure 13.

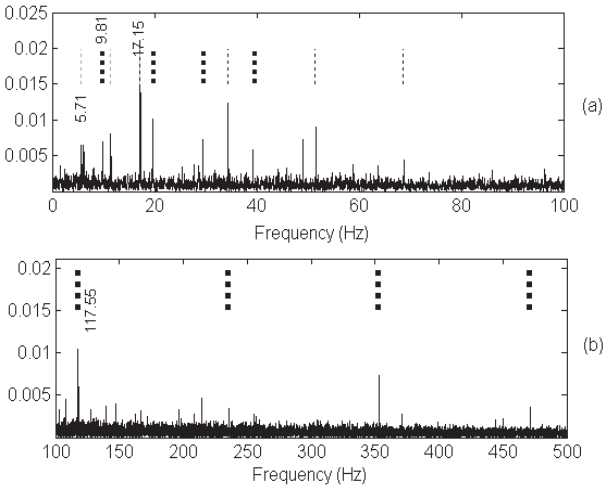

Figure 14: SK automated envelope analysis (a) squared envelope spectrum (0-100 Hz) (b) squared envelope spectrum (100-400 Hz).

This will help identify the source of the impacts in the signal by comparing the detected frequencies with those earlier presented in tables 2 and 3 for gears and bearings respectively. Note the impulsive nature of the squared envelope.

For more insight into the source of the frequencies, figure 14 looks at two frequency regions of the squared envelope spectrum (namely from 0-100 Hz in figure 14a, and from 100-400 Hz in figure 14b). The frequencies originating from the gears and their harmonics are presented by thin harmonic cursor, while those relating to one of the frequencies in table 5.5 (defect bearing frequencies) are presented by a thick harmonic cursor.

For the gears, it is shown that the planet pass frequency of 17.21 Hz (three times the carrier frequency (5.71 Hz) strongly dominates the lower part of the spectrum. The 9.81 Hz and the 117.76 Hz components strongly match the FTF and the BPFI of the planetary gear bearings respectively. This strongly indicates that the planetary bearing is defective. The fact that the BPFI is present indicates a damaged inner race, while modulation by the cage frequency indicates differences between the rolling elements, which would often result from defective elements.

4 PROGNOSTICS AND FAULT SEVERITY INDICATORS

One of the key issues in bearing prognostics is the ability to detect the defect in its incipient stages, which in turn gives enough time to track its development and avoid any catastrophic failure. SK armed with recent optimisations and enhancements gives a clear separation of the signal arising from a bearing defect, and thus is ideal for being implemented in prognostic models. It gave a good measure of the severity of the fault when compared to the amount of metal wear debris in the oil (figure 15).

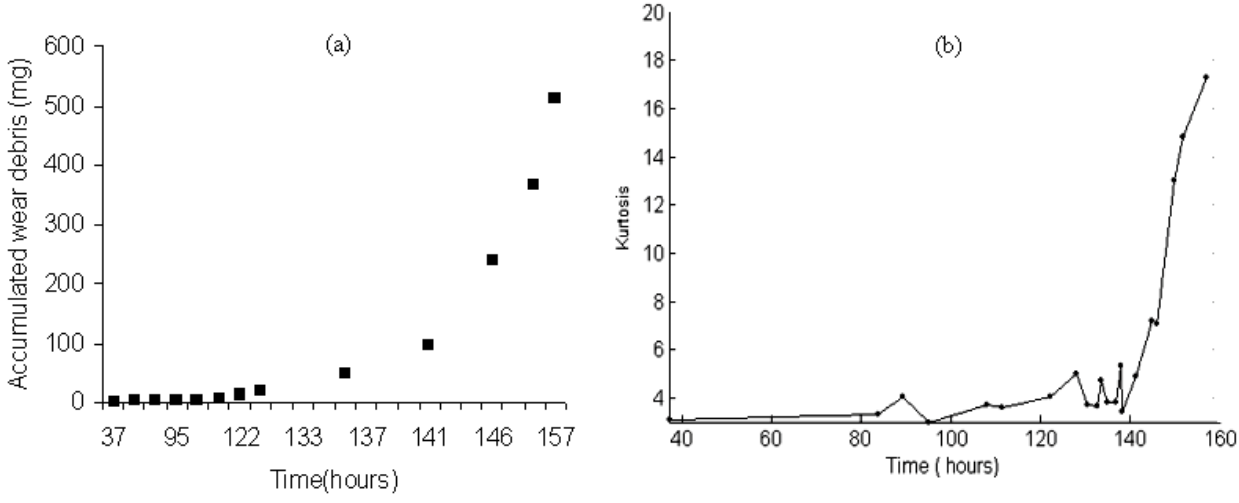

Figure 15: Helicopter gearbox trends. (a) Accumulated metal wear debris. (b) Kurtosis of the filtered signal.

Constant percentage bandwidth (CPB) comparisons were also performed to see how the fault severity is tracked using this technique. In the CPB analysis, as the name suggests, spectra used for comparisons are of constant percentage bandwidth (CPB), rather than of constant bandwidth and cover a wide frequency range of three decades. Figure 16 shows a 3D plot of the CPB comparisons (linear frequency scale), showing where the most excited bands are, and how this evolves with time ie as the bearing condition gets worse. A clear increase of the dB difference is seen around 18 kHz frequency (which matches the results earlier presented through the analysis of SK). However, neither the values, nor the pattern indicates the severity sensed by the accumulated mass of wear detected in the oil, or the increase in the envelope spectrum as presented in the diagnostic section between the start of the test and the final measurement. A significant change is normally 6 dB or more. The CPB spectrum comparison gave a weak indication of the deterioration but could not be considered significant. There was also little change in the temperature of the oil (figure 17).

5 FAULT INSPECTION AND VERIFYING THE FINDINGS

A very good result was achieved for the analysis of the test data. The fault was in one of the planet gear support bearings as has been indicated in the analysis (figure 18a). Furthermore there was damage to the inner race (figure 18b) correctly identified, and to the rolling elements as well (figure 18c). The fault, which developed in the inner race and the rolling elements, showed its signature clearly in the envelope spectrum through the harmonics of the inner race pass frequency, which were modulated by the load variation frequency in the last stages, indicating severe damage. SK gave an excellent measure of the severity of the fault and the bearing degradation process was clearly represented by its evolution. Other tested parameters for severity analysis such as CPB analysis and vibration statistics of the raw signal gave little indication of the fault. There was also little change in the temperature of the oil. The end result of the processing algorithm (envelope spectrum) contains all the necessary information and the whole algorithm can be automated for a complete

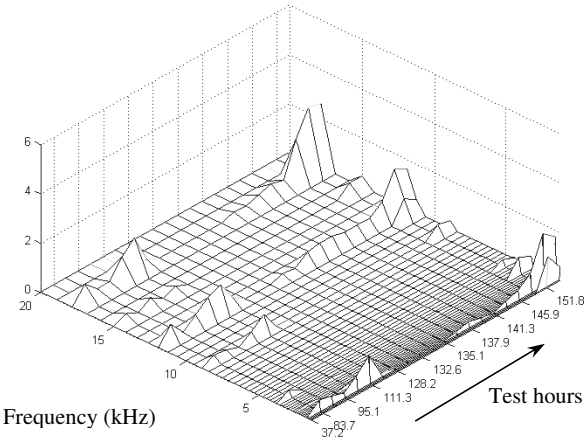

Figure 16: Constant Percentage Bandwidth (dB) – Reference measurements at hour 37.2.

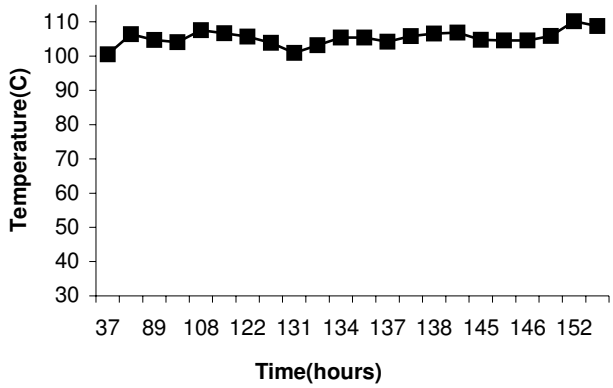

Figure 17: Oil temperature variations as test proceeded.

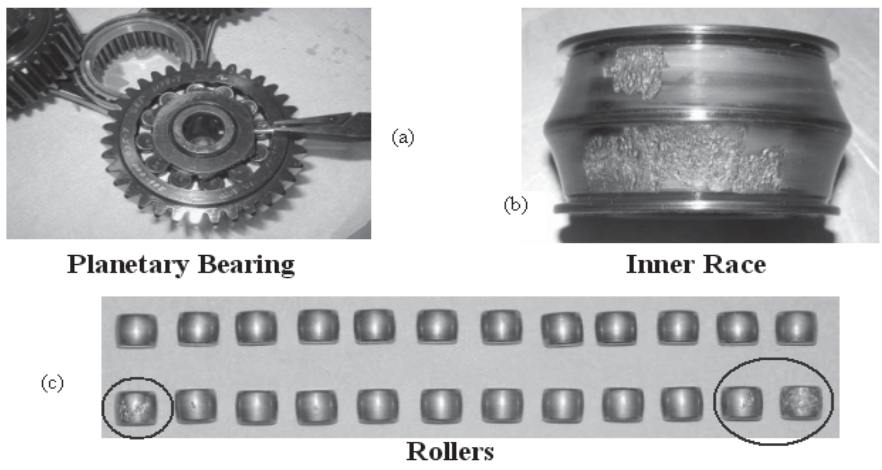

Figure 18: (a) defective bearing, (b) spalled inner race (c) defective rollers.

identification of any bearing related faults. This is in contrast to the traditional diagnostic techniques, which require the analyst to select a suitable band for performing the envelope analysis (requires historical data or can be done by trial and error), and may need more than one position to measure at.

6 CONCLUSIONS

The presented processing algorithm needs minimal user interference to remove the strong gear signal and to determine the suitable band for the envelope analysis. No historical data is required and one sensor would be enough to detect faults in most cases. The presented processing algorithm for detecting faults in rolling element bearings is in fact an easy and effective tool that requires minimal interference and experience from the user. The algorithm is not only able to detect faults in noisy and awkward situations in a clear way but also is capable of tracking the fault severity.

ACKNOWLEDGEMENTS

This work is supported by the Australian Defence Science and Technology Organisation (DSTO) as a part of their Centre of Expertise scheme.

REFERENCES

Akaike, H. 1969, "Fitting autoregressive for prediction", Ann.Inst.Math, Vol. 21, pp. 243-247.

Antoni, J. & Randall, R. B. 2004, "Unsupervised noise cancellation for vibration signals: part 2-A Novel Frequency Domain Algorithm", *Mechanical Systems and Signal Processing*, Vol. 18, No. 1, pp. 103-118.

Antoni, J. & Randall, R. B. 2006, "The Spectral kurtosis: Application to the Surveillance and Diagnostics of Rotating Machines", *Mechanical Systems and Signal Processing*, Vol. 20, No. 2, pp. 308-331.

Antoni, J. 2006, "The Spectral kurtosis: A useful tool for characterising nonstationary signals", *Mechanical Systems and Signal Processing*, Vol. 20, No. 2, pp. 282-307.

Bonnardot, F., Randall, R. B. & Antoni, J. 2004, "Enhanced unsupervised noise cancellation using angular resampling for planetary bearing fault diagnosis", *International Journal of Acoustics and Vibration*, Vol. 9, No. 2.

Darlow, M. S., Badgley, R. H. & Hogg, G. W. 1974, "Application of high frequency resonance techniques for bearing diagnostics in helicopter gearboxes", *US Army Air Mobility Research and Development Laboratory Technical Report*, pp. 74-77.

Dempsey, P., Lewicki, D. & Decker, H. 2004, "Transmission bearing damage detection using decision fusion analysis", *NASA technical paper*, NASA/TM-2004-213382.

Forrester, B. D. 1991, "Time-frequency domain analysis of helicopter transmission vibration", Department of Defence, Aeronautical Research Laboratory, *Propulsion Report 180*.

Ho, D. & Randall, R. B. 2000, "Optimisation of bearing diagnostic techniques using simulated and actual bearing fault signals", *Mechanical Systems and Signal Processing*, Vol. 14, No. 5, pp. 763-788.

Howard, I. 1994, "A review of rolling element bearing vibration: detection, diagnosis and prognosis", *DSTOAMRL report*, DSTO-RR-00113, pp. 35-41.

Huff, E. & Tumer, I. 2003, "Using triaxial accelerometer data for vibration monitoring of helicopter gearboxes", *Journal of Vibration and Acoustics*, Vol. 128, No. 4, pp. 120-128.

Joanes, D. N. & Gill, C. A. 1998, "Comparing measures of sample skewness and kurtosis", *Journal of the Royal Statistical Society (Series D): The Statistician*, Vol. 47, No. 1, pp. 183-189.

Lang, G. 1999, "S&V geometry 101", *Sound and vibration*, pp. 1-12.

Lewicki, D. & Coy, J. 1987, "Vibration characteristics of OH58a helicopter main rotor transmission", *NASA technical paper*, NASA TP-2705/AVSCOM TR 86-C-42.

McFadden, P. D. & Howard, I. M. 1999, "The detection of seeded faults in an epicyclic gearbox by signal averaging of the vibration", Department of Defence, Aeronautical Research laboratory, *Propulsion Report 183*.

McFadden, P. D. & Smith, J. D. 1985, "An explanation for the asymmetry of the modulation sidebands about the tooth meshing frequency in epicyclic gear vibration", *Proceedings of the Institution of Mechanical Engineers*, 199(C1), pp. 65-70.

Sawalhi, N. & Randall, R. B. 2005, "Spectral kurtosis enhancement using autoregressive models", *The 4th Australasian Congress on Applied Mechanics*, Melbourne.

Sawalhi, N. & Randall, R. B. 2005, "Spectral kurtosis optimization for rolling element bearings", *8th International Symposium on Signal Processing and Applications*, Sydney.

Wang, W. & Wong, A. K. 2002, "Autoregressive model-based gear fault diagnosis", *Transaction of ASME, Journal of Vibration and Acoustics*, Vol. 124, pp. 172-179.

NADER SAWALHI

Nader Sawalhi was born in Canberra, Australia in 1974. He received the BSc degree in mechanical engineering from the University of Jordan, Amman, Jordan in 1997. He received the MEngSc degree and the PhD in 2001 and 2007 respectively, both in mechanical engineering, from the University of New South Wales (UNSW), Sydney, Australia.

Between 1997 and 2003, he was with Jordan Cement Factories, Amman, Jordan, as a reliability and predictive maintenance engineer. From 2003 to 2007 he worked on his PhD project at UNSW developing signal processing algorithms and simulation models for rolling element bearings in complex environments. The project, under the supervision of Prof Bob Randall, was fully supported by the Australian Defence Science and Technology Organisation (DSTO) as a part of their Centre of Expertise scheme. He spent three months on a sponsored internship with FAG Bearings, Schweinfurt, Germany, in 2004. Since 2007 he has been working at the School of Mechanical and Manufacturing Engineering at UNSW as a Research Associate. His research interests include signal processing, machine condition monitoring, diagnostics and prognostics.

Dr Sawalhi is a member of the Jordanian Engineering Association and is eligible for membership of Engineers Australia.

BOB RANDALL

Bob Randall is a Professor in the School of Mechanical and Manufacturing Engineering at the University of New South Wales, Sydney, Australia. He has a degree in mechanical engineering from the University of Adelaide, and an Arts degree in mathematics and Swedish from the University of Melbourne. Prior to joining the University in 1988 as a Senior Lecturer he worked for the Danish company Bruel & Kjaer for 17 years where he was responsible for developing systems for machine condition monitoring and diagnostics. He previously had ten years' experience in the chemical and rubber industries in Australia, Canada and Sweden. He was promoted to Associate Professor in 1996 and to Professor in 2001. He is the author and/or co-author of the Bruel & Kjaer books Frequency Analysis and Mechanical Vibration and Shock Measurements, and the invited author of chapters on vibration measurement and analysis in the McGraw-Hill handbooks *Shock and Vibration Handbook* and *Handbook of Acoustical Measurements and Noise Control* as well as the *Encyclopedia of Vibration* (Academic Press), and the forthcoming *Handbook of Noise and Vibration Control* (Wiley). He was invited to contribute a chapter on "Signal Processing in Vibration Analysis", in *Structural Dynamics @ 2000: current status and future directions*, (Eds. D.J. Ewins and D.J. Inman) Research Studies Press. He is a member of the editorial board of the journals *Mechanical Systems and Signal Processing* and *The International Journal of Comadem*. He is the author of more than 140 papers in the fields of vibration analysis and machine diagnostics, and has successfully supervised eleven PhD and three Masters projects in these areas. He is the Director of the DSTO Centre of Expertise in Helicopter Structures and Diagnostics located at the University of NSW, one of four such Centres of Expertise set up and funded in Australian universities by DSTO (Defence Science and Technology Organisation). The main function of the Centre has been to carry out research into diagnostics of helicopter gearboxes and gas turbines, as well as the structural dynamics of helicopter airframes.